remote sensing

Article

Real-Time Terrain Correction of Satellite Imagery-Based Solar Irradiance Maps Using Precomputed Data and Memory Optimization

Myeongchan Oh, Chang Ki Kim, Boyoung Kim, Yongheack Kang and Hyun-Goo Kim *

Renewable Energy Big Data Laboratory, Korea Institute of Energy Research, Daejeon 34129, Republic of Korea; amir117@kier.re.kr (M.O.)
* Correspondence: hyungoo@kier.re.kr

Abstract: Satellite imagery-based solar irradiance mapping studies are essential for large-scale solar energy assessments but are limited in spatial resolution and accuracy. Despite efforts to increase map resolution by correcting inaccuracies caused by shadows on the terrain, the computational time of these models and the massive volume of generated data still pose challenges. Particularly, forecasting generates large amounts of time series data, and the data production rate is faster than the computational speed of traditional terrain correction. Moreover, while previous research has been conducted to expedite computations, a novel and innovative technology in terrain correction is still required. Therefore, we propose a new correction method that can bypass complex calculations and process enormous data within seconds. This model extends the lookup table concept, optimizes the results of many shadow operations, and stores them in memory for use. The model enabled 90 m scale computations across Korea within seconds on a local desktop computer. Optimization was performed based on domain knowledge to reduce the required memory to a realistic level. A quantitative analysis of computation time was also conducted, revealing a previously overlooked computational bottleneck. In conclusion, the developed model enables real-time terrain correction and subsequent processing of massive amounts of data.

Keywords: solar radiation; solar irradiance; terrain; shadowing; shading; high-resolution

Citation: Oh, M.; Kim, C.K.; Kim, B.; Kang, Y.; Kim, H.-G. Real-Time Terrain Correction of Satellite Imagery-Based Solar Irradiance Maps Using Precomputed Data and Memory Optimization. *Remote Sens.* **2023**, *15*, 3965. https://doi.org/10.3390/rs15163965

Academic Editor: Filomena Romano

Received: 27 June 2023
Revised: 2 August 2023
Accepted: 8 August 2023
Published: 10 August 2023

1. Introduction

Research on solar irradiance mapping has been widely conducted for various purposes, such as site selection and planning. Solar irradiance maps generally focus on a large area and use satellite images to estimate the national solar irradiance distribution [1–3]. As these maps require continuous weather data feed, a geostationary satellite with low spatial resolution continuously observes an area, enabling the acquisition of a solar irradiance map with a spatial resolution on the kilometer scale. However, even the most advanced satellite has a 0.5 km resolution for a single band in a visible channel, and when other band images are used to calculate irradiance, a lower resolution is obtained. In addition, satellite-driven solar maps do not account for shadows or shading from the terrain. Therefore, various methods of terrain correction have been explored to increase spatial resolution while also considering the influence of the terrain [4–9].

The fundamental algorithm for shadow correction is intuitive, and many equations describing it were proposed before the 1990s [4]. Since then, numerous studies have attempted to increase the computational efficiency or accuracy of this algorithm using various methods, such as vectorial algebra [5], validation [6,7,9], and a modified model for cloudy conditions [8]. However, despite these efforts, the amount of computation required by the algorithm has not yet been overcome. Currently, even with reduced computation time, large areas require minutes to hours of computation [10–15]. While this may not pose an issue for values that require one-time computation, it becomes a significant problem for values requiring continuous computation. In this study, the former and latter are categorized as static and dynamic values, respectively, and are summarized in Table 1.

As terrain features do not change, they are often referred to as static boundary conditions [16]. In contrast, delineating features such as shadows, which change with the position of the sun, as invariant is challenging. Values unrelated to the position of the sun are referred to as static values in the present study. Static values, such as the sky view factor (SVF) [4], do not need to be recomputed. However, dynamic values related to the position of the sun, such as shadows for direct irradiance, must be calculated in every case. Therefore, dynamic values change with the position of the sun and need to be calculated at every time and location. Calculating both values is easy when performing shadow calculation on only one point, as the precalculated horizontal height of nearby terrain can be used. However, it is difficult to apply such a calculated horizon for large areas.

Dynamic values, which require only one azimuth to be considered, are dozens of times faster than static values; however, they still require a few minutes for computation. As data production cycles decrease and the need for terrain correction over large areas increases, the computation time problem becomes more pronounced. Additionally, the wide solar resource map service requires many of these computations to be performed in real-time. In particular, forecasting with shadow correction requires extensive calculations because it generates multiple solar maps in each forecast horizon. Currently, several maps in service [17,18] display the results of applied terrain correction; however, the existing technology does not allow for real-time calculations.

A limited number of quantitative studies on improving the speed of terrain corrections have been conducted. These studies mainly focused on the computation time for static values, which require longer computation time. Romero et al. [10] have performed rapid shadow calculations for a clear sky using azimuthal sector division and showed that approximately 1 h is required for an area of 4500 × 4500. Oh and Park [11] analyzed the calculation time and complexity according to shadow calculation models and showed that the time required for an area of 900 × 900 was 20 min. Some studies [12–15] have focused on computational hardware, especially graphics processing units (GPUs), for rapid calculation. Tabik et al. [12] advanced a previous study [10] and proposed a new model with precalculation and a parallel algorithm; they obtained the fastest calculation time of 2.5 s for 500 points (sites). Strendardo et al. [15] obtained a calculation time of 1–2 h for 6800 × 6800 high-resolution maps using a GPU. These studies showed that minutes to hours are required to calculate shadows for an area with a size of thousands × thousands. Although other studies have devised a new index [19] or applied machine learning [20,21] for faster calculations, they could only approximate annual values and not accurately determine time series results.

This computational load increases with spatial and temporal resolutions [11]. Regardless of improvements in the current computing technologies, if the amount of data to be processed increases, its calculation speed cannot keep up without innovative technology. In terms of satellite images, recent weather satellites, such as the GEO-KOMPSAT-2A (GK-2A), generate images every two minutes, indicating that solar maps are modeled and transmitted every two minutes. If the calculation speed falls behind, data will accumulate and processing becomes challenging. In addition, adequate preparation for managing higher resolutions and enormous data in the future is necessary.

Many studies on shadow calculations have focused on buildings in urban areas [13–15] and not on the terrain because calculations for buildings require substantial computation per calculation. As these studies include large datasets, the need for high levels of computation has been steadily increasing. However, terrain correction that does not consider buildings also encounters computational challenges when the area is extended to a national scale. The algorithms for shadow calculations are similar for terrains and urban areas but differ in detailed factors. Algorithms for terrains include the difference between the position of the sun and the irradiance according to the region. In contrast, those for urban areas should include the irradiance on vertical façades and complex modern structures.

Technically, factors obtained by interpolation may be more important for terrains than for urban areas. Although the present study focused on terrains, the basic concepts of shadows are equally applicable.

Despite its importance in terrain correction, interpolation is overlooked in many studies. Matching irradiance to high-resolution terrain data inevitably requires an increase in spatial resolution. Interpolation is a suitable approach to address these spatial differences; however, it needs to be optimized in terms of accuracy and computation time. In terms of accuracy, interpolation for solar irradiance has been well-investigated [22–24]. However, most of these previous studies have attempted to interpolate between measurement stations that are spaced hundreds of kilometers or more apart. Moreover, although weather-based irradiance is not expected to have a significant impact on interpolation accuracy on a grid larger than 1 km, the calculation time has not been well investigated and can be an important issue in real-time calculations, such as those used in the present study. Real-time terrain corrections require frequent interpolation, which can reduce efficiency as it is time-consuming. Therefore, a quantitative analysis of this aspect is warranted to comprehensively assess its effects on the overall performance of real-time terrain corrections.

In this study, we aimed to quantitatively evaluate the calculation time of terrain correction and subsequently propose a new model for a faster application. This model was devised to bypass the demanding computation process, enabling the estimation of real-time shadow corrections possible for satellite-based solar maps. The proposed model does not compromise the accuracy of the existing model as it utilizes the results of the existing calculation. Moreover, by bypassing calculation, the model can store and apply the calculation results in advance. We also analyzed memory optimizations for actual conduction and additional factors that pose challenges in real-time computation, such as the interpolation process. In addition, we quantitatively identified and compared data, computing power, model efficiency, and memory requirements. Through testing and verification, we determined that the data produced every few minutes could be processed within a few seconds on a general desktop without depending on a supercomputer. The necessity and objectives of this study are presented in Figure 1.

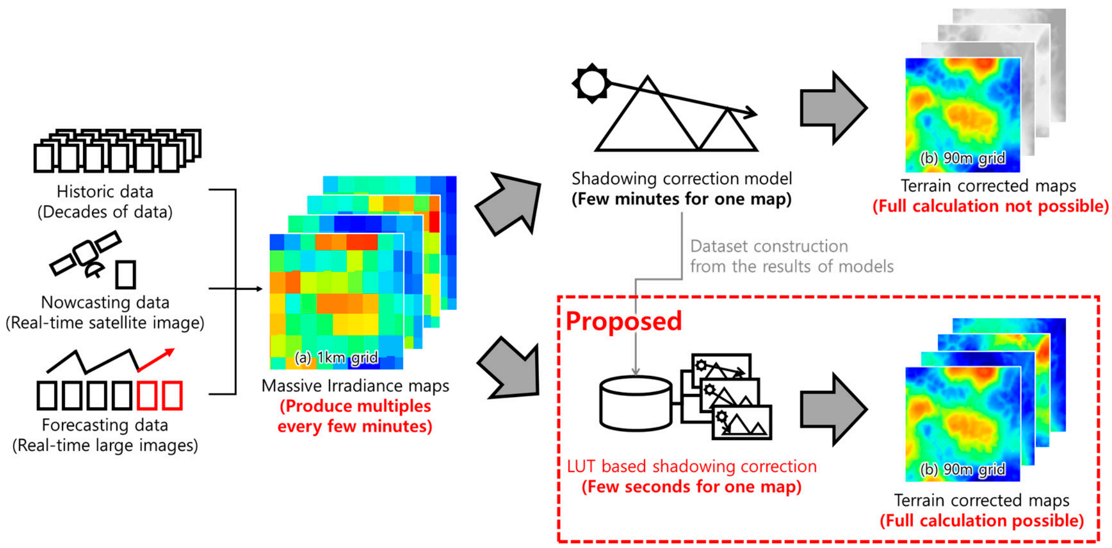

Figure 1. Necessity and objectives of the study. Abbreviation: LUT, lookup table.

Table 1. Comparison of static and dynamic values for terrain correction.

Algorithm Category	Required Calculations	Changes According to the Sun's Position	Examples	Each Calculation Time
Static	Once	X	SVF, DHI ratio, etc.	High
Dynamic	Every case	O	Shadows, DNI ratio, etc.	Relatively low

Abbreviations: DHI, diffuse horizontal irradiance; DNI, direct normal irradiance.

2. Materials and Methods

2.1. Data

2.1.1. Low-Resolution Solar Irradiance Maps

Real-time satellite-derived solar irradiance maps were generated by the Korea Institute of Energy Research using the UASIBS-KIER model [1,25]. This model can extract both global and direct irradiance from satellite images. The Communication, Ocean, and Meteorological Satellite (COMS) was used before 2020 in version one (v1) of the model, whereas the next-generation meteorological satellite, GK-2A, was used after 2020 inversion two (v2) of the model. UASIBS-KIER v1 [25] with the COMS and v2 with GK-2A [1] had spatial resolutions of 1 km and 0.5 km and temporal resolutions of 15 min and 2 min, respectively, for the entire territory of Korea. The correction model proposed in this study can be applied to both model results. The latest data of the v1 model with low resolution, obtained in 2019, were used to maximize the effect of correction. The size of the maps from UASIBS-KIER v1 was 636 × 459.

2.1.2. High-Resolution Terrain Maps

Terrain data with a spatial resolution of 90 m, namely the digital elevation model (DEM), were acquired from the National Geographic Information Institute (Gyeonggi-do, Republic of Korea). The difference between high-resolution terrain maps and low-resolution solar maps is approximately 10 times in one dimension and 100 times in the area. The actual visual differences are shown in Figure 1a,b. The coordinate system used in this study was the universal transverse Mercator (UTM)-K system, which is a correction of the UTM coordinate system to match Korea. The final product was produced according to high-resolution terrain data; thus, low-resolution data were used only for the location and value of the initial data. The DEM was constructed for the entire area of South Korea and had a size of 6816 × 7147. However, part of the eastern area was removed because it mainly comprised sea; therefore, a final size of 6816 × 5000 was used. As this area is a peninsula, and terrain correction is unnecessary for the rest of the sea, approximately 50% of the actual terrain was considered.

2.2. Shadow Calculation Algorithms

Many studies have been conducted to calculate the shadowing of terrain. The calculation of shadows created by direct irradiance occlusion is intuitive and simple. However, estimating the shadows for diffuse irradiance is difficult. Previous methods for shadow calculation are summarized and compared in this section.

2.2.1. Equations and Numerical Calculations

The determination of total irradiance requires the calculation of both beam and diffuse irradiances (Figure 2). Each of these can be measured and used as values of direct normal irradiance (DNI) and diffuse horizontal irradiance (DHI), which provide quantitative values for the solar component of beam irradiance and the horizontal component of diffuse irradiance, respectively. The total irradiance can be expressed as the sum of these two irradiances, particularly in the horizontal direction, and is termed global horizontal irradiance (GHI). In some studies, reflected irradiance has been included in the total irradiance; however, the present study did not consider it because it requires additional variables, such as albedo. The shadowing effect of DNI becomes zero when it is covered and has no effect otherwise. Therefore, it can be easily calculated by mathematically comparing the altitude angle of the sun and that of the terrain, as shown in Equation (1) [7].

$$\hat{B} = \begin{cases} B & (\varepsilon_S^{\varnothing_S} > \varepsilon_T^{\varnothing_S}) \\ 0 & (\varepsilon_S^{\varnothing_S} \le \varepsilon_T^{\varnothing_S}) \end{cases} \quad (1)$$

$\hat{B}$ denotes the DNI with a shadowing effect, B denotes the DNI, $\varnothing_S$ denotes the azimuth angle of the sun, $\varepsilon_S^{\varnothing_S}$ denotes the altitude angle of the sun according to its azimuth angle, and $\varepsilon_T^{\varnothing_S}$ denotes the altitude angle of the terrain according to the azimuth angle of the sun. The angle variables are shown in Figure 3. A weight of 0.5 can be given to the equation if all the angles are the same.

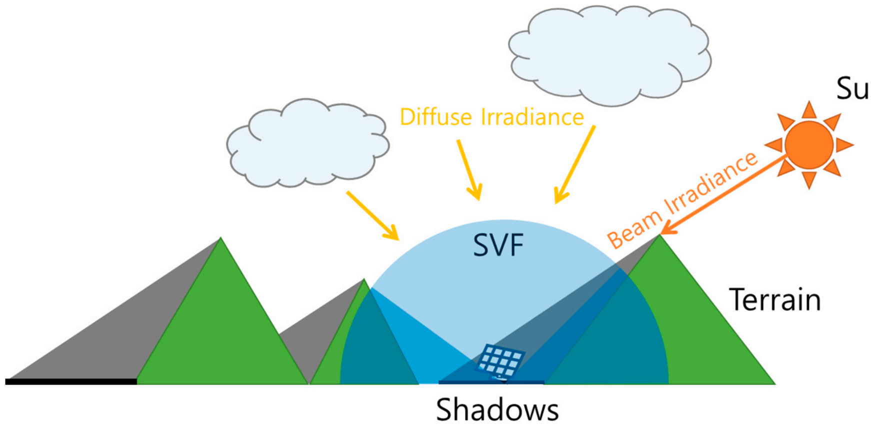

Figure 2. Schematic diagram of solar irradiance and shadows according to the position of the sun. Abbreviations: SVF, sky view factor.

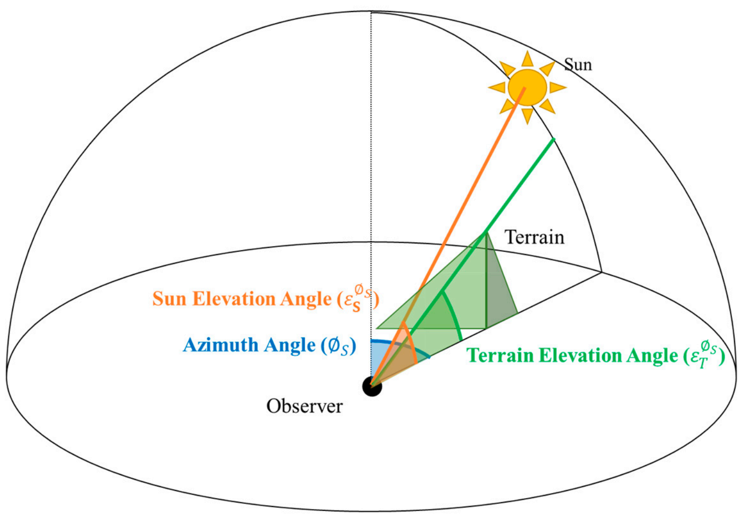

Figure 3. Schematic diagram of the angle variables related to the sun and terrain.

In the case of DHI, the influence of shadows was calculated as a continuous value rather than 0 and 1. The most popular method for this is the SVF method, which estimates shadows caused by surrounding sky obstruction with the assumption of isotropic diffusion [4]. As this method assumes isotropy, every sky obstruction has the same weight; thus, shadows can be easily calculated by obtaining the ratio of obstruction to the total sky area

(SVF). Equations (2) and (3) show the calculation of SVF [26]. An alternative method, which uses a distribution of diffused irradiance and sky obstruction, has been proposed [27] and used in the ArcGIS Solar Analyst toolbox. However, many studies have preferred the SVF method because of its simplicity.

$$SVF = \frac{1}{2\pi}\int_0^{2\pi}\left[\cos\theta_P \sin^2\theta_T^{\varnothing} + \sin\theta_P\cos(\varnothing - \varnothing_P) \times \left(\theta_T^{\varnothing} - \sin\theta_T^{\varnothing}\cos\theta_T^{\varnothing}\right)\right]d\varnothing \quad (2)$$

$$\hat{D} = SVF \times D \quad (3)$$

where θ_P denotes the zenith (tilt) angle of the surface, $\theta_T^{\varnothing}$ denotes the zenith angle of the terrain according to the azimuth angle, $\varnothing_P$ denotes the azimuth angle of the surface, $\hat{D}$ denotes the DHI with shadowing effect, and D denotes the DHI. The sum of the zenith and altitude angles is 90°.

DNI and DHI can be extracted from the physical model or separated using separation models. This study used both irradiances from the UASIBS-KIER model. However, additional processes were conducted for diffuse irradiance division and irradiance on a tilted surface. A previous terrain correction study [7] divided diffuse irradiance into two types: circumsolar and isotropic. As circumsolar diffuse irradiance is similar to direct irradiance; it is comparable to a direct irradiance with 0 and 1 shadowing. The Perez model [28] is the most widely used model for diffuse irradiance division; thus, we applied it in our study. In addition, irradiance on a tilted surface can be calculated based on the Perez model. Direct irradiance (including circumsolar irradiance) on a slope can be calculated by considering the angle, and isotropic diffuse irradiance can be calculated as the sky hemisphere decreases. However, this process must be considered along with the shadow calculation because the decrease in the sky hemisphere due to slope and terrain can overlap (Figure 4).

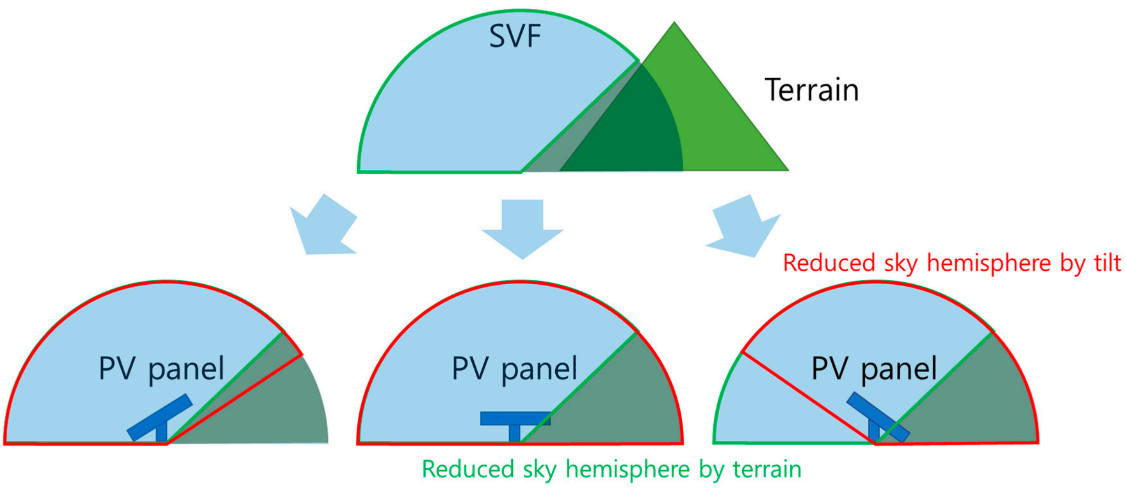

Figure 4. Schematic diagram of the relationship between terrain and sky view factor (SVF). As they can overlap with one another, calculating them separately and considering their overlap is necessary. Abbreviations: PV, photovoltaic.

Although the shadowing of both direct and diffuse irradiance can be estimated by equation, calculating every case according to the position of the sun or integrating over large terrain areas is difficult. Moreover, the calculation of terrain zenith angles and their integration is considerably challenging for a large area. Thus, numerical analysis-based calculations can be used to improve the efficiency of this process [29]. This digitization can be conducted using terrain data and the sky. The DEM is generally used as discrete topography data, which converts Equation (2) from an integral to a summation. The sky hemisphere can also be digitized by zenith and azimuth angles or other criteria [30]. Moreover, a previous study has shown that division by angle is advantageous in terms of calculation efficiency [11]; this lattice makes the calculations simple and fast.

2.2.2. Regional Calculations

The problem of the computational load becomes more significant when the shadowing effect of an entire region is estimated. Estimating shadows for only one site is relatively easy, whereas that at every location requires extensive computation. Moreover, shadows from direct irradiance require calculations that are relatively straightforward but must be calculated separately according to the time or position of the sun. Therefore, many approaches have attempted to calculate these spatiotemporal shadows simultaneously. Some studies simultaneously estimated shadows for an entire area (shadow-based calculation) and others simultaneously estimated shadows for an entire time period (viewmap-based calculation) [11]. However, for the former, the calculation becomes more complex when the area is considerably large due to variations in the sun's position across the area. Thus, the latter approach is used to consider the position of the sun in each location. Moreover, although the estimation of shadows from diffuse irradiance requires only one value for each time point, it requires significant calculations at each location. Thus, many studies have attempted to rapidly estimate SVF for large areas using various approaches, such as pyramid datasets and GPU processes [15].

Estimating the horizon height according to the azimuth angle is essential for both shadow calculations. Horizon height refers to the height of the terrain in each azimuth direction in the sky, which can be converted to a sky coverage map, which was called a viewmap, viewshed, skyshed, or shading mask in previous studies. Both shadow effects can be easily calculated using this horizon height; however, it is the most extensive step of the entire calculation. Its minimum time complexity is $O(n^2 \log(n))$ [11] for an area of size $n \times n$, and the total calculation time exponentially increases as the area increases. In the present study, the *r.horizon* function in the open-source GRASS GIS 7.8.4 software was used to calculate the horizon height, which took over 20 h of calculation time for an area of 7000×5000 on a local desktop. Therefore, applying the existing method to real-time terrain corrections is not appropriate.

An additional problem for regional calculation is spatial interpolation. Before shadow correction, aligning the low-resolution irradiance map with the high-resolution topographical data is necessary. However, this process requires a considerable amount of time to calibrate over a large area. When the *griddata* function in the *SciPy* library was applied for interpolation, an area of 7000×5000 required approximately 40 s of computational time on a local desktop. Performing calculations in real-time and for many forecast horizons is challenging with this calculation time. Additionally, constructing the correction result for multiple variables, including tilted and direct irradiance, requires a significantly longer time.

2.2.3. Calculation Process and Lookup Table

The overall terrain correction process is shown in Figure 5. Deviations may exist depending on the model, but most models follow a similar structure. In the case of solar position calculations, the position of the sun according to parallax should be considered for national-scale research. Calculating the solar position in all areas requires a considerable amount of time; however, it could be bypassed by interpolation after calculating the solar positions of some locations. Thus, the most time-consuming part of the process is the calculation of the shadows and SVF. The horizon height algorithm can be used for both processes; however, horizon calculation for only the sun's azimuth direction is needed for shadow calculation. Spatial interpolation should be conducted for low-resolution solar maps, including direct and diffuse irradiance and the cosine of the zenith angle of the sun. Interpolation was time-consuming because the other procedures required relatively little time, excluding the calculation of horizon height.

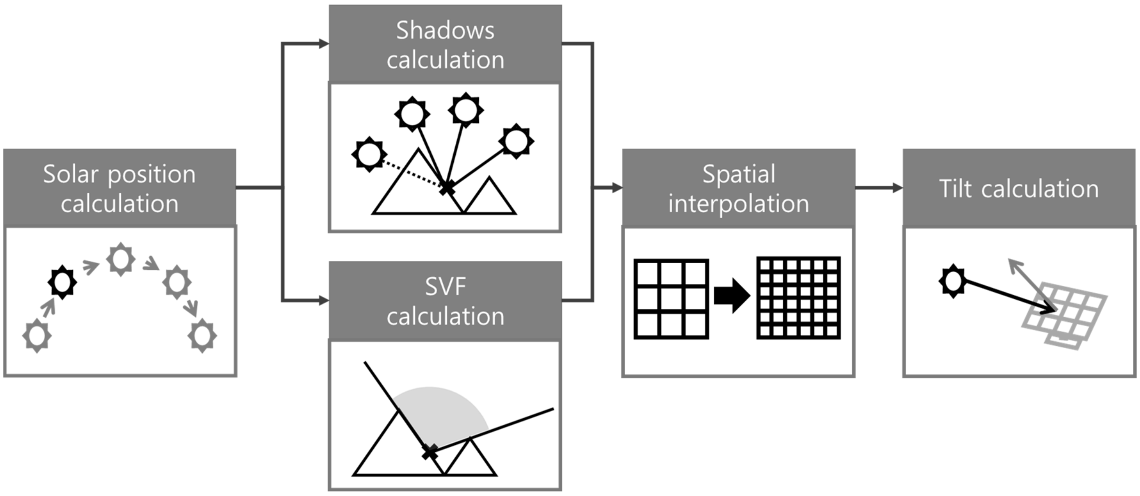

Figure 5. Simplified flowchart of terrain correction for large areas.

Although applying the same algorithm to multiple spacetimes is easy, applying it in physical time is considerably difficult. In this respect, many studies have been conducted to reduce the amount of computation, and the most fundamental method is to reduce the time complexity of the algorithms. Although a previous study has reduced this time complexity [11], the real-time process requires a more drastic time reduction and a fundamental change. One of these efficient methods, namely the lookup table (LUT), is used to make a table of existing precalculated results and load them without calculation. Based on this concept, our study devised a new processing model that performs terrain correction in a time complexity of O(1). Constant time complexity indicates that the computation time does not increase as the resolution or scope increases; all operations can be performed quickly regardless of the time complexity of the algorithms. The computation time can be substantially reduced by simplifying the high-computation process. However, considering the memory requirements of the process is necessary. In particular, precalculated data must be used in random-access memory (RAM) rather than storage, such as hard disk drives (HDD) and solid-state drives (SSD). Although SSD is faster than HDD, it is still 10–100 times slower than RAM. Table 2 summarizes the calculation methods: equation-based, numerical, and LUT-based.

Table 2. Summary of the different calculation methods and their features.

Calculation Method	Direct (Beam) Irradiance Shadowing	Diffuse Irradiance Shadowing	Point Calculation	Regional Calculation	Required Memory
Equation	Fast	Difficult	Fast	Very difficult	Low
Numerical	Fast	Slow	Fast	Very slow	Medium
Lookup table	Fast	Fast	Fast	Fast	High

2.3. *Proposed Real-Time Calculation Model*

2.3.1. Lookup Table-Based Dataset Composition

The original LUT has one value for each key; however, the dataset in this study had a map for each key. Four types of maps were stored and used in the dataset: shadow, SVF, DNI ratio, and DHI ratio maps. The shadow map is a binary-type map containing information on the shadows from direct irradiance. The SVF map was used to calculate SVF values at each location. The DNI ratio (cosine of the angle between the position of the sun and the slope at each location) and DHI ratio (the coverage area of the sky hemisphere, considering both terrain and slope) maps were used to estimate the tilted irradiance. As the shadow and DNI ratio maps changed according to the position of the sun, they were calculated and stored for each position of the sun in the sky grid, which required large amounts of storage. In contrast, the SVF and DHI ratio maps required the calculation and storage of only one map. Figure 6 shows the composition of the LUT-based dataset.

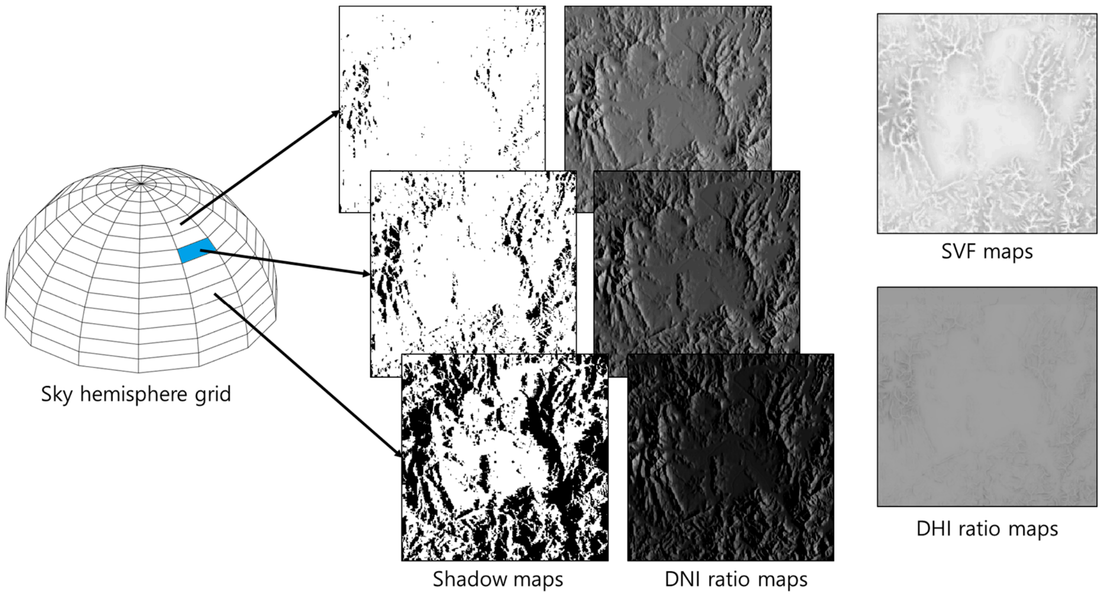

Figure 6. Schematic diagram of the structure and indexing of the proposed lookup table-based dataset. Abbreviations: DNI, direct normal irradiance; SVF, sky view factor; DHI, diffuse horizontal irradiance.

Constructing a dataset of maps according to the position of the sun is intuitive and convenient. However, its application becomes difficult when the location of the sun differs depending on the region. Therefore, this study selected a reference position to calculate the position of the sun as well as its relative position in other regions. In other words, the dataset was constructed according to the reference position of the sun rather than its actual position. This approach of shadow calculation is equivalent to considering the curvature of the entire Earth. Although this difference appears to be marginal, it enables the calculation of a large area without errors possible from solar time.

2.3.2. Fast Interpolation Method

Interpolation can be a bottleneck in computation (validated in Section 3.3); therefore, the efficiency of the interpolation method must be improved. As interpolation is a common method in many fields, increasing the calculation speed by modifying the fundamental algorithm is difficult. However, increasing efficiency by eliminating repetitive processes is possible and is similar to LUT-based methods. The interpolation process requires the construction of an interpolant by triangulating the input data [31]. As the data here had the same location as the low-resolution data and high-resolution area, every interpolation process had the same interpolant. Thus, the entire process could be accelerated by removing the iterative interpolant operation. Specifically, the same operations in *Delaunay grid generation*, *triangulation searching*, *and barycentric coordination calculation* functions in *griddata* in the *SciPy* library can be removed. The calculation speed can be improved by approximately 10 times by removing these repetitive parts. In the results section, we quantitatively measure and compare the calculation time of the old and new interpolation methods. Faster interpolation, such as simple filling, is possible when accuracy is severely sacrificed, but this case was not considered.

2.3.3. Memory Optimization

The optimization of capacity is essential for using all LUT datasets in RAM. As shadow and DNI ratio maps were generated according to the position of the sun, an increase in the sky hemisphere grid number also increased the required memory. Therefore, selecting an appropriate resolution level was important. A previous study [11] has shown that the number of azimuth and zenith angles below 60 and 10, respectively, can significantly reduce accuracy. However, the method based on the shadow map showed good accuracy even when the number of azimuth angles was 20. In addition, our study used azimuth and zenith angles of 36 and 10, respectively. This resolution can be modified according to the results and the actual physical system.

The LUT dataset requires at least twice as much map data as sky grids. Therefore, the case study had hundreds of maps with a size of 7000 × 5000. Assuming that the number of each map was in the 64-bit float data format of 8 bytes, the capacity of each map was 280 MB. When the number of these maps was 360 (sky grid number) × 2 + 2 = 722, the total capacity was over 200 GB, which is generally impractical to store in RAM. Additional sets were required to compute multiple slopes. Accordingly, several techniques were used to compress capacity. (1) Maps for all sky hemisphere areas were not required. Shadow correction only required maps of the areas where the sun passes, especially where a shadow is cast. Therefore, determining the ratio of the shadowed area was necessary, and the capacity could be reduced accordingly. However, additional processing for indexing was required in this case because the LUT key cannot be in the form of a two-dimensional grid. (2) The shadow map contained only 0 and 1 values, which could have a format of 1 byte Boolean, which could reduce the total capacity by approximately half to an eighth of its original size. The actual capacity and feasibility were analyzed by constructing a LUT dataset for Korea. (3) Finally, areas that do not require terrain correction were excluded. In cases where the study area included a considerable amount of sea, such areas were removed. However, this process required changing the maps to one-dimensional arrays and constructing an index to retrieve them.

2.4. Methodology

This study focused on data-setting and real-time computing of terrain correction, not the algorithm itself. Therefore, a methodology to verify them was designed and implemented (Figure 7). First, we reviewed terrain correction to ensure its accuracy. The results were validated by testing a sample of maps and a time series data of selected sites. Next, the composition and capacity of the built dataset were analyzed. Lastly, finally, the calculation time of terrain correction was measured for each procedure.

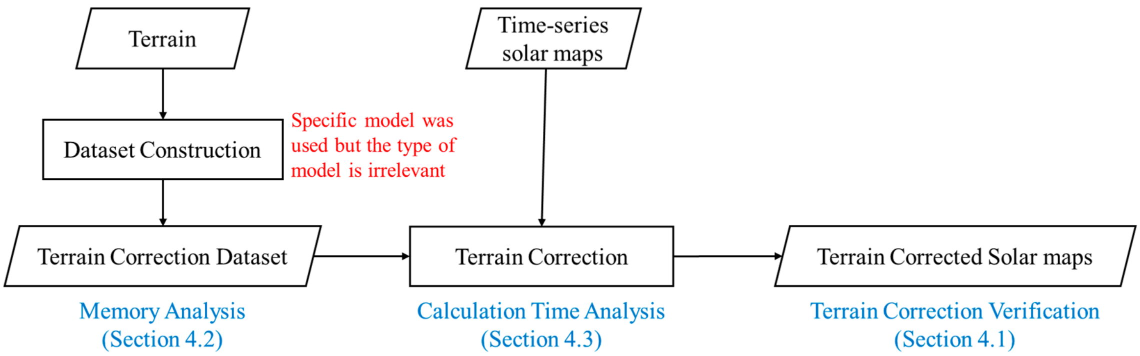

Figure 7. Flowchart of the study methodology.

2.4.1. Terrain Correction Verification

First, terrain correction results were rudimentarily validated based on visualization results. The evaluation focused on whether each procedure calculated the appropriate results and whether there were any errors in the domain knowledge base. In particular, since there is interpolation in the procedure, the interpolation and terrain correction results were visualized and evaluated separately. Second, the time series patterns of the equation-based correction and the proposed model correction results were analyzed for randomly selected sites. The selected sites and their location, terrain, and horizon height are visualized in Figure 8. Six sites with shading areas with more than 20% by terrain were selected. In time series validation, both cases use the same solar irradiance and horizon height, with the only difference being the real-time calculation versus a LUT dataset. For accuracy, there is a marginal variation due to how the sun's position is calculated.

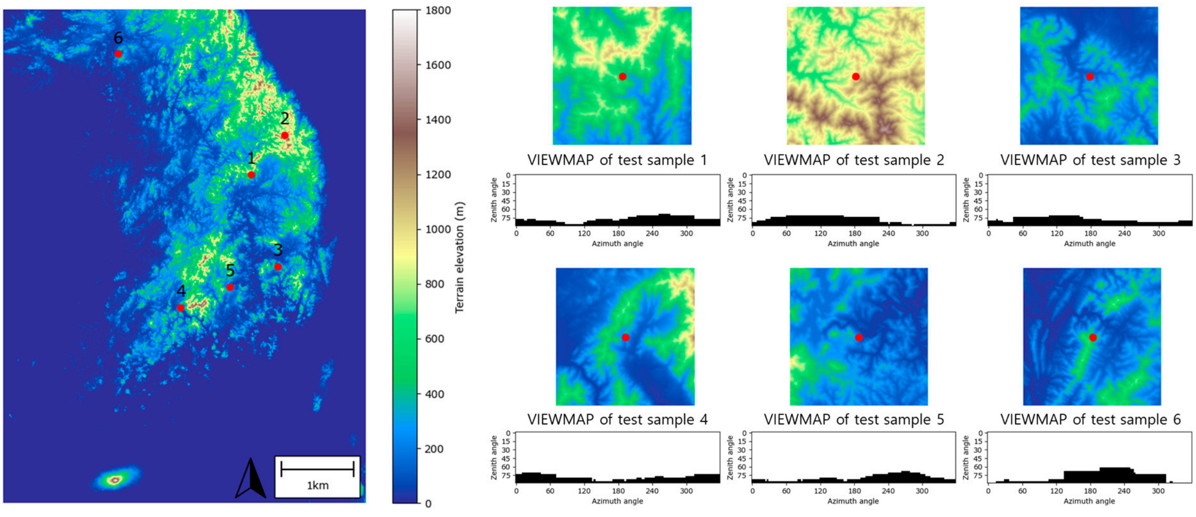

(a) **(b)**

Figure 8. (**a**) Distribution of six randomly selected sites for validation and (**b**) the nearby terrain elevation and corresponding horizon height (viewmap) of each site.

Terrain correction was conducted based on a numerical model, and a LUT dataset was built from the results. The numerical model and dataset construction extended the model from the author's previous study [11,32] and were designed and conducted in MATLAB R2021a. Subsequently, terrain correction was conducted in Python 3.10 using the dataset for the time series satellite-based solar maps. The dataset was constructed in mat format and used in Python through the *HDF5 for Python (h5py)* library. The formula-based correction in the sample test used *Python* to calculate the sun position at each location and each time to perform the correction.

2.4.2. Memory Analysis

Memory analysis was conducted based on the theoretical capacity calculated in Section 2.4 and the measured capacity. The before and after capacities were compared with theoretical calculations for each of the three proposed capacity reduction techniques. Additionally, the effective position of the sun for the first capacity reduction technique was visualized. The possibility of applying terrain correction using only RAM memory was also investigated.

2.4.3. Calculation Time Analysis

Calculation time was measured based on the procedure in Figure 5. The difference in calculation time between the ordinary and proposed models was compared and the time taken by each procedure was also visualized. The measurements were conducted by performing calculations in MATLAB, Python, and QGIS. The computing machine was a local desktop with an i9-10900 KF 3.70 GHz CPU and DDR4 64 GB RAM. Windows 10 software was used as the operating system. Multithreading was conducted in MATLAB using the *parfor* function; however, multithreading or GPU acceleration was not used in the other models.

3. Results

3.1. Terrain Correction

Figure 9 shows an example of the terrain correction process and the visualized results. The results of the numerical calculation and LUT dataset were similar, and the only difference was the calculation time and memory usage. The figure shows clear differences between the raw and the corrected maps. Irradiance refers to GHI, and the tilted irradiance is calculated based on the slope direction of the terrain. The terrain slope direction was selected as the tilted surface for a clear comparison of the results. However, in this example, there is no shadow of direct irradiance; therefore, only irradiance decreases due to SVF are shown. These aspects were confirmed on the 1-year cumulative map, as shown in Figure 10. The influence of the terrain that was not visible on the raw satellite irradiance map was clearly confirmed after terrain correction. The effect of the terrain aspect can be confirmed in the tilted irradiance results.

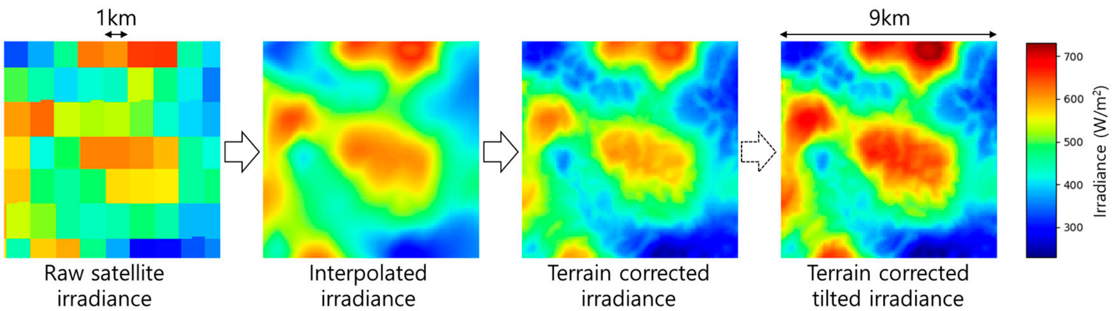

Figure 9. Example of the terrain correction process applied to the instantaneous satellite-based solar map at a specific time.

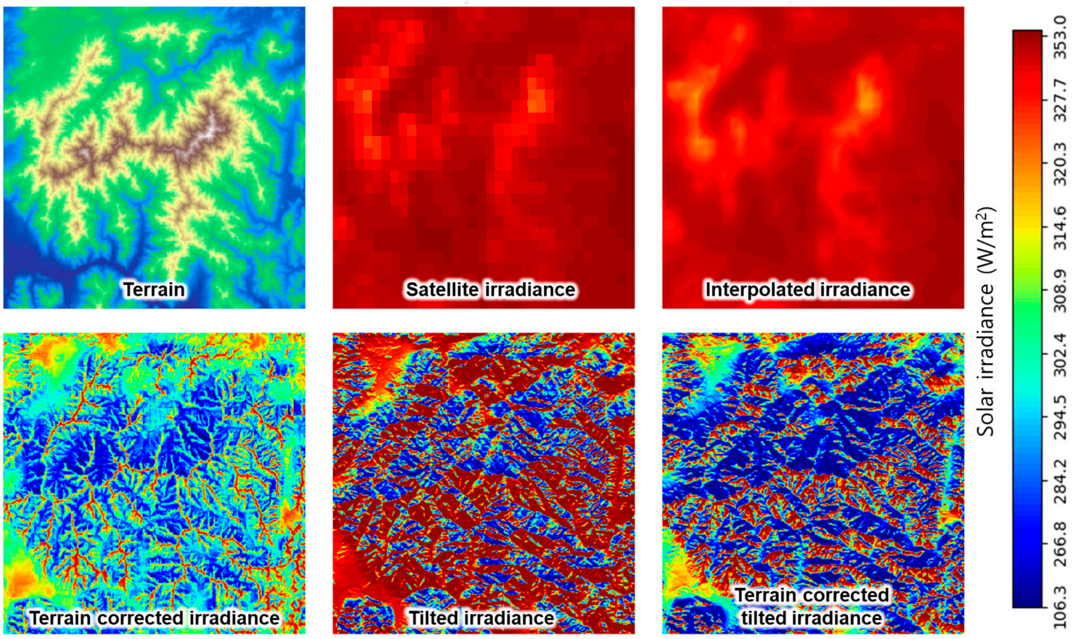

Figure 10. Comparison of the satellite-based solar map before and after terrain correction at a specific region. This is the result of the 1-year accumulated map.

Examples of time series patterns before and after terrain correction for the six selected sites are shown in Figure 11. These patterns were calculated over a single day and a significant decrease in GHI after terrain correction was observed for most sites. The results of the model using the equation-based and the precomputed results are almost identical, with only a slight difference because the proposed model used the sun's position based on the value of the reference point. As a result, when comparing the correction results over a 10-day sample period for the six sites, the root mean squared error (RMSE) was 10–50 W/m^2. The relatively high errors were primarily caused by differences in the calculation of occlusion when direct irradiance was high. These errors may be reduced by increasing the grid resolution.

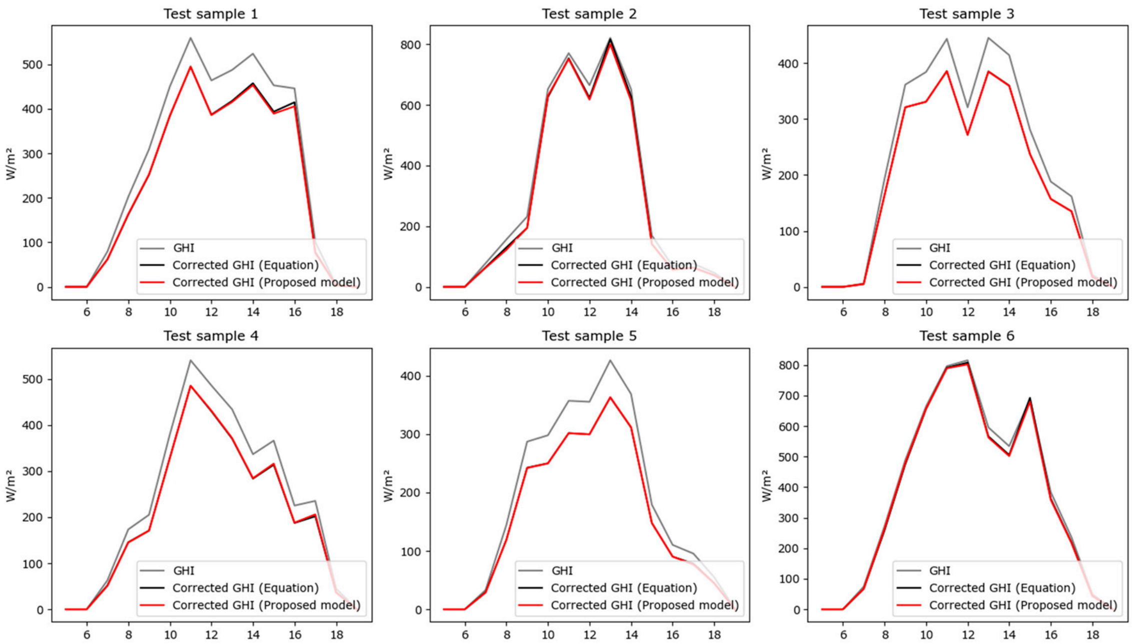

Figure 11. Examples of time series patterns before and after terrain correction for six sites. Both equation-based and proposed models for terrain correction are shown.

3.2. Required Memory and Optimization

The LUT dataset had a total memory of approximately 10 GB, which is sufficient for RAM use. The dataset was constructed for a 6816 × 5000 area with a 20 × 36 sky hemisphere grid and one tilted slope. Three capacity reduction techniques were applied: (1) valid position of the sun, (2) data type, and (3) excluded area. Only 33% of the sky grid area showed a valid sun position and only 52% had shadows. Figure 12 shows the areas in the sky grid with the valid position of the sun. Among the valid positions of the sun, 48% of the area was shadow-free and 83% had less than 1% shadow coverage. Consequently, 83% of the memory can be reduced using the first technique. In the second technique, 44% of the capacity ((1 + 1/8)/2) can be reduced in theory, but an additional capacity reduction is possible if a 32-bit float is used. Finally, as this study included large sea areas, the capacity could be reduced by 49%, and the theoretical memory capacity of 200 GB could be reduced to 5%.

3.3. Calculation Time

The calculation times were measured for each process, as shown in Figure 13. Figure 13a shows an ordinary process with calculations for each location and Figure 13b shows the process without static values calculations. Figure 13c shows the proposed model results. The horizon height calculation algorithm with the pyramid dataset was 20 times faster than that using *GRASS GIS*, but it still required an hour. Despite the large area of 7000 × 5000, most processes except for solar position calculation, horizon height calculation, and interpolation could be resolved within 1 s. In addition, among the three processes that required considerable time, the first two processes were replaced with the LUT dataset, and it was confirmed that the change took less than 1 s. The position of the sun was also not an issue because only the reference point needed to be calculated due to the composition of the dataset.

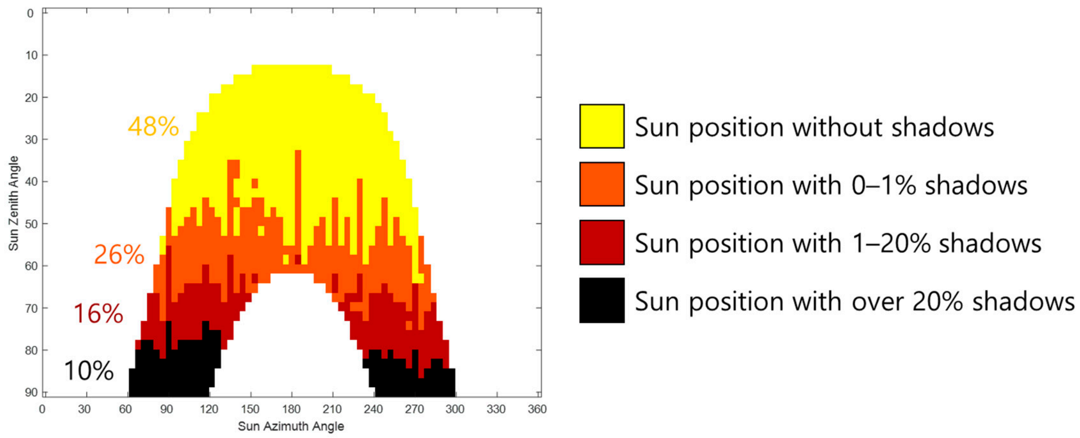

Figure 12. Areas in the sky grid with valid positions of the sun along with their percentages of shadows.

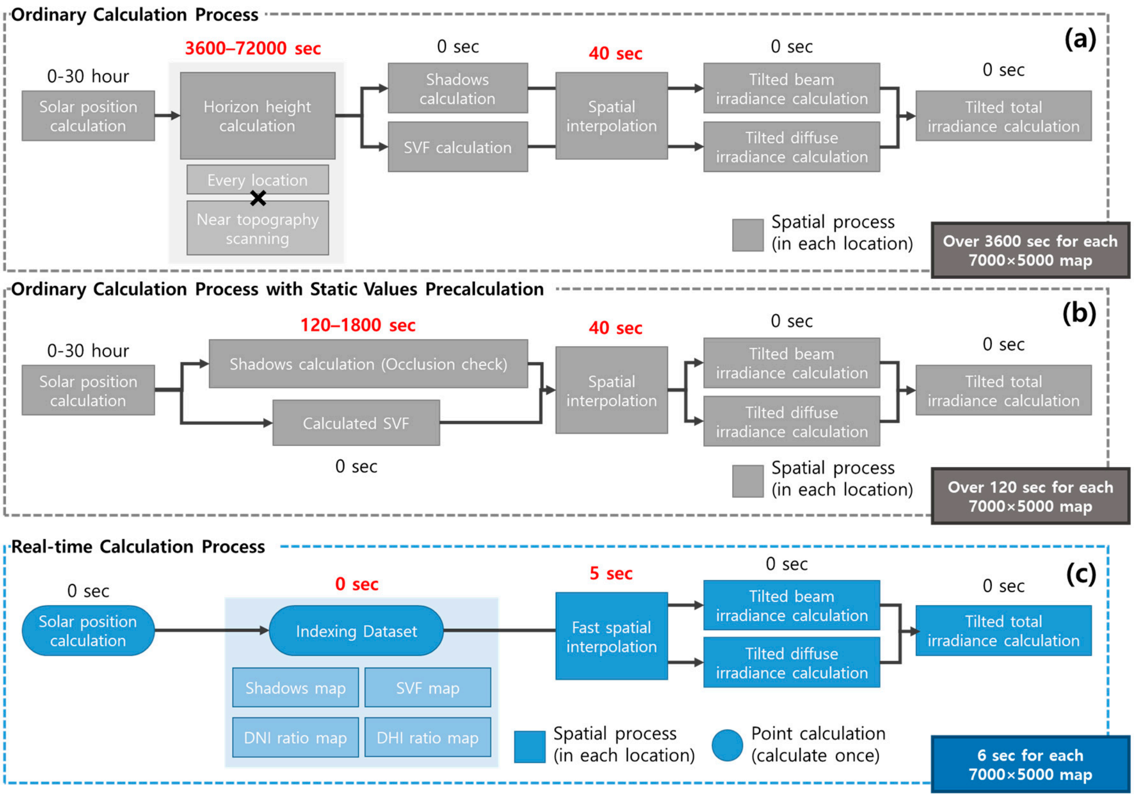

Figure 13. Flow chart and calculation time for the (**a**) ordinary, (**b**) ordinary with static values precalculation, and (**c**) proposed real-time calculation models. Abbreviations: SVF, sky view factor; DNI, direct normal irradiance; DHI, diffuse horizontal irradiance.

Interpolation required approximately 13 s per map using the old method and under 2 s using the new method. This result indicates that the simple application of traditional interpolation is inefficient because it involves repetitive work. Interpolation needs to be applied to at least two maps each time, DNI and DHI. In this study, interpolation was applied to three maps, including the cosine value of the zenith angle for GHI computation. As a result, the existing interpolation method required at least 40 s of calculation time for interpolation alone, whereas the new method allowed for the interpolation to be performed in 5 s. In the new model, shadow computation, which was originally time-consuming, was computed in less than a second, and most of the total process time was spent on interpolation.

Table 3 lists the calculation times of the models. The four models in the table are the existing numerical model, the optimized numerical model, the modified model using the LUT, and the final model of this study. The time required for one satellite-based solar map was reduced from 20 h to 6 s. Regardless of the optimization of the existing numerical analysis model, it could not correspond to the latest satellite images at 2 min intervals. The time for processing 1 year of past data based on UASIBS-KIER v1 at 15 min intervals was also estimated. Numerical models could not process such data without distributed computing, but the proposed new model quickly processed the entire year within 2 days. In terms of forecasting, when forecasting was performed based on satellite imagery at 2 min intervals, terrain correction was possible in more than 10 forecast horizons.

Table 3. The calculation time of the different terrain correction models.

	Calculation Time for One Satellite-Based Solar Map (s)	Calculation Time for Processing 1 Year of Past Data with 15 Min Intervals (h)
GRASS GIS r.horizon	70,000 (20 h)	400,000 (43 years)
VIEWMAP with the pyramid dataset	4000 (1 h)	20,000 (2 years)
LUT-based dataset	40	210
LUT DB + Fast interpolation model	6	32

Abbreviations: LUT, lookup table; DB, database.

4. Discussion

4.1. Application of Fast Terrain Correction

The proposed model can generate terrain-corrected solar maps for an area within seconds. It was optimized for application in instantaneous solar maps from satellite images and numerical weather predictions. However, this model is not efficient for estimating annual irradiance and evaluating the potential in a new area. Hundreds of these maps are generated daily, and performing terrain correction on each one was not feasible with previous models. If computational resources are retained after the correction of real-time data, they can be applied to historical data. Accordingly, high-resolution long-term solar data can also be extracted. However, storing such high-resolution time series data requires considerable capacity. This huge amount of storage requirement can be saved if data can be generated whenever needed based on fast calculations. When fast computation is possible, various applications, resource savings, and decision-making based on economic feasibility also become possible.

Fast calculation technology is essential for the operation of energy digital twins or smart cities, which require substantial computation. Over the past 10 years, thousands of studies related to energy digital twins have been conducted [33]. In particular, owing to the influence of buildings on cities, many studies on digital twins in urban areas have been proposed [34,35]. Accurate irradiances must be used in these models, and input variables must be calculated quickly for operation. As mentioned in the introduction, shadow correction for terrain and buildings is similar and has many common characteristics. Therefore, the model proposed in this paper can also be applied to urban shadow correction. Although additional methods for building façades and three-dimensional objects should be devised, the basic concept of fast calculation is still valid. If real-time shadow calculation based on this study is performed, this digital twin technology is expected to provide an opportunity to advance.

4.2. Influence of Terrain Correction

Assessing the economic impact of terrain correction is the easiest approach to explaining its influence. Previous studies have accounted for this by calculating the change in decision-making [36] or economic value [37] of using research findings in the marketplace. An approach to calculate similar results for this study is to compare the results before and after terrain correction. Figure 14 shows the one-year cumulative solar irradiance before and after terrain correction. The mean annual solar irradiance in the study area showed a reduction of approximately 6%, which can have a considerable impact on the economic analysis and can potentially determine the feasibility of the project. In addition, more than 10% of the area lost more than 10% of its shadows. Such spatial patterns must be estimated to increase the accuracy of solar irradiance and photovoltaic power. The pattern is distinctly different not only in small areas (as shown in Figure 10), but also in large areas. Another important issue is the influence on the time series patterns; real-time patterns are important for power plant operation, and shadows can change these patterns. Based on the patterns shown in Figure 11, the difference between the time series patterns before and after terrain correction for the six sites is 7–18% RMSE, which can have devastating consequences for forecast accuracy and impact the forecast market.

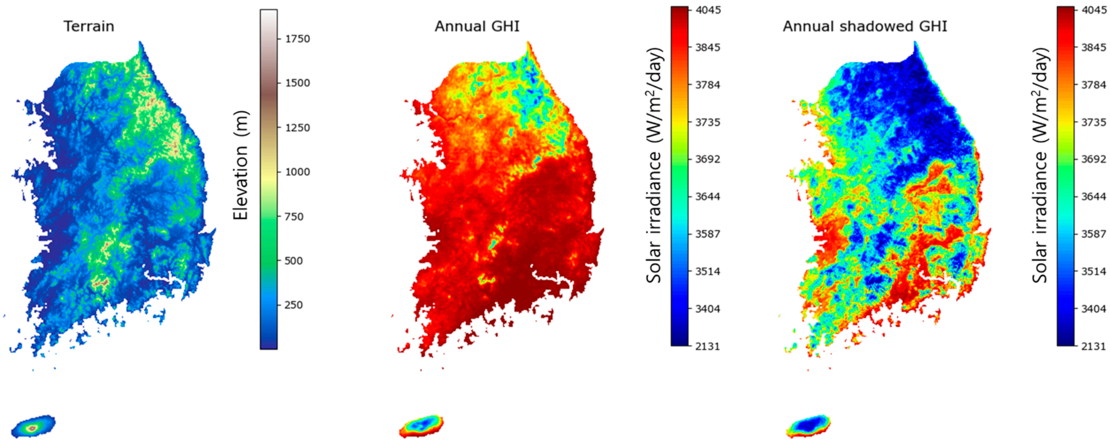

Figure 14. Comparison of a solar map of South Korea before and after terrain correction. GHI, global horizontal irradiance.

4.3. Accuracy of the Model

Accuracy can be an issue when developing faster, lightweight models. In this study, the equation-based and proposed model results were applied to some sites and compared. The results revealed only a marginal difference between the two models. The present study excluded the impact of differences in the resolution of terrain or the underlying models used to calculate the influence of terrain because they are either irrelevant or have been previously studied [16]. Accuracy issues based on the computational model are irrelevant as any model can be applied to this study. The model used in this study utilizes the results of existing models; hence, every model can be used. Accuracy according to resolutions has already been addressed [11]; the resolutions that affect accuracy are terrain resolution and sky hemisphere grid number, and their accuracy analysis on a model similar to that used in our study has been reported [11]. The resolution of the terrain is already determined by the data, and as we utilized the highest-level data in the present study, the resolution is not a point of concern. Moreover, accuracy is highly dependent on the division of the azimuth, and the azimuth can be increased further depending on the accuracy level required. In our study, a relatively small value of 36 was used as the number of azimuth divisions to analyze multiple cases and validate their feasibility on a local desktop. However, this number can be easily increased, and the memory required grows linearly with resolution. We have excluded these aspects from the main part of the paper because estimating the required memory and possibilities based on the results is easy.

5. Conclusions

The necessity for terrain correction on solar maps has been emphasized, and various studies have been conducted accordingly. Nevertheless, the amount of data has increased faster than the development of algorithms, and the processing of accumulated and real-time data has become considerably challenging as a result. Therefore, this study proposed a semi-real-time operation through systematic dataset construction rather than a simple enhancement of the efficiency of the algorithm. Our approach allows for terrain correction for a wide area within seconds using a local desktop. We verified our approach by conducting quantitative research on memory and calculation speed, revealing previously overlooked factors, such as interpolation time, which were discovered and resolved in the process. In the future, real-time calculations are expected to be feasible if a large-scale server or distributed computing is used. This study may serve as a foundation for the establishment of new directions for existing studies and pave the way for exploring new possibilities in real-time corrections of satellite imagery.

Author Contributions: Conceptualization, M.O.; methodology, M.O.; software, M.O. and C.K.K.; validation, B.K.; investigation, C.K.K. and B.K.; resources, C.K.K.; data curation, C.K.K. and B.K.; writing—original draft preparation, M.O.; writing—review and editing, H.-G.K.; visualization, M.O.; supervision, Y.K. and H.-G.K.; project administration, H.-G.K.; funding acquisition, H.-G.K. All authors have read and agreed to the published version of the manuscript.

Funding: This work was conducted under the framework of the research and development program of the Korea Institute of Energy Research (C3-2412).

Data Availability Statement: The data presented in this study are available upon request from the corresponding authors. The data are not publicly available because of the restrictions.

Conflicts of Interest: The authors declare no conflict of interest.

References

1. Kim, C.K.; Kim, H.G.; Kang, Y.H.; Yun, C.Y.; Lee, Y.G. Intercomparison of satellite-derived solar irradiance from the GEO-KOMSAT-2A and HIMAWARI-8/9 satellites by the evaluation with ground observations. *Remote Sens.* **2020**, *12*, 2149. [CrossRef]
2. Huang, G.; Li, Z.; Li, X.; Liang, S.; Yang, K.; Wang, D.; Zhang, Y. Estimating surface solar irradiance from satellites: Past, present, and future perspectives. *Remote Sens. Environ.* **2019**, *233*, 111371. [CrossRef]
3. Perez, R.; Ineichen, P.; Moore, K.; Kmiecik, M.; Chain, C.; George, R.; Vignola, F. A new operational model for satellite-derived irradiances: Description and validation. *Sol. Energy* **2002**, *73*, 307–317. [CrossRef]
4. Dubayah, R.; Rich, P.M. Topographic Solar-Radiation Models for Gis. *Int. J. Geogr. Inf. Sci.* **1995**, *9*, 405–419. [CrossRef]
5. Corripio, J.G. Vectorial algebra algorithms for calculating terrain parameters from dems and solar radiation modelling in mountainous terrain. *Int. J. Geogr. Inf. Sci.* **2003**, *17*, 1–23. [CrossRef]
6. Bosch, J.L.; Batlles, F.J.; Zarzalejo, L.F.; López, G. Solar resources estimation combining digital terrain models and satellite images techniques. *Renew. Energy* **2010**, *35*, 2853–2861. [CrossRef]
7. Ruiz-Arias, J.A.; Cebecauer, T.; Tovar-Pescador, J.; Šúri, M. Spatial disaggregation of satellite-derived irradiance using a high-resolution digital elevation model. *Sol. Energy* **2010**, *84*, 1644–1657. [CrossRef]
8. Zhang, S.; Li, X.; She, J.; Peng, X. Assimilating remote sensing data into GIS-based all sky solar radiation modeling for mountain terrain. *Remote Sens. Environ.* **2019**, *231*, 111239. [CrossRef]
9. Ma, Y.; He, T.; Liang, S.; Mcvicar, T.R.; Hao, D.; Liu, T.; Jiang, B. Estimation of fine spatial resolution all-sky surface net shortwave radiation over mountainous terrain from Landsat 8 and Sentinel-2 data. *Remote Sens. Environ.* **2023**, *285*, 113364. [CrossRef]
10. Romero, L.F.; Tabik, S.; Vías, J.M.; Zapata, E.L. Fast clear-sky solar irradiation computation for very large digital elevation models. *Comput. Phys. Commun.* **2008**, *178*, 800–808. [CrossRef]
11. Oh, M.; Park, H.D. A new algorithm using a pyramid dataset for calculating shadowing in solar potential mapping. *Renew. Energy* **2018**, *126*, 465–474. [CrossRef]
12. Tabik, S.; Villegas, A.; Zapata, E.L.; Romero, L.F. A fast GIS-tool to compute the maximum solar energy on very large terrains. *Procedia Comput. Sci.* **2012**, *9*, 364–372. [CrossRef]
13. Lukač, N.; Žalik, B. GPU-based roofs' solar potential estimation using LiDAR data. *Comput. Geosci.* **2013**, *52*, 34–41. [CrossRef]

14. Huang, Y.; Chen, Z.; Wu, B.; Chen, L.; Mao, W.; Zhao, F.; Wu, J.; Wu, J.; Yu, B. Estimating roof solar energy potential in the downtown area using a GPU-accelerated solar radiation model and airborne LiDAR data. *Remote Sens.* **2015**, *7*, 17212–17233. [CrossRef]
15. Stendardo, N.; Desthieux, G.; Abdennadher, N.; Gallinelli, P. GPU-enabled shadow casting for solar potential estimation in large urban areas. Application to the solar cadaster of Greater Geneva. *Appl. Sci.* **2020**, *10*, 5361. [CrossRef]
16. Geraldi, E.; Larosa, S.; Romano, F.; Cersosimo, A.; Cimini, D.; Di Paola, F.; Gallucci, D.; Gentile, S.; Nilo, S.T.; Ricciardelli, E.; et al. The analysis of static boundary condition in solar resource assessment by satellite: The role of high-resolution Digital Terrain Model in irradiance downscaling process. In Proceedings of the 4th International Conference on Energy & Meteorology (ICEM), Bari, Italy, 27–29 June 2017.
17. Šúri, M.; Huld, T.A.; Dunlop, E.D. PV-GIS: A web-based solar radiation database for the calculation of PV potential in Europe. *Int. J. Sustain. Energy* **2005**, *24*, 55–67. [CrossRef]
18. Suri, M.; Cebecauer, T. *SolarGIS: New Web Based Service Offering Solar Radiation Data and Tools for Europe, North Africa and Middle East*; International Solar Energy Society: Freiburg im Breisgau, Germany, 2016; pp. 1–7.
19. Calcabrini, A.; Ziar, H.; Isabella, O.; Zeman, M. A simplified skyline-based method for estimating the annual solar energy potential in urban environments. *Nat. Energy* **2019**, *4*, 206–215. [CrossRef]
20. Vartholomaios, A. A machine learning approach to modelling solar irradiation of urban and terrain 3D models. *Comput. Environ. Urban Syst.* **2019**, *78*, 101387. [CrossRef]
21. Lin, S.; Chen, N.; Zhou, Q.; Lin, T.; Li, H. A Scheme for Quickly Simulating Extraterrestrial Solar Radiation over Complex Terrain on a Large Spatial-Temporal Span—A Case Study over the Entirety of China. *Remote Sens.* **2022**, *14*, 1753. [CrossRef]
22. Şen, Z.; Şahin, A.D. Spatial interpolation and estimation of solar irradiation by cumulative semivariograms. *Sol. Energy* **2001**, *71*, 11–21. [CrossRef]
23. Chelbi, M.; Gagnon, Y.; Waewsak, J. Solar radiation mapping using sunshine duration-based models and interpolation techniques: Application to Tunisia. *Energy Convers. Manag.* **2015**, *101*, 203–215. [CrossRef]
24. Leirvik, T.; Yuan, M. A Machine Learning Technique for Spatial Interpolation of Solar Radiation Observations. *Earth Space Sci.* **2021**, *8*, 1–22. [CrossRef]
25. Kim, C.K.; Kim, H.G.; Kang, Y.H.; Yun, C.Y. Toward Improved Solar Irradiance Forecasts: Comparison of the Global Horizontal Irradiances Derived from the COMS Satellite Imagery Over the Korean Peninsula. *Pure Appl. Geophys.* **2017**, *174*, 2773–2792. [CrossRef]
26. Dozier, J. Rapid Calculation of Terin Parameters for Radiation Modeling From Digital Elevation Data. *IEEE Trans. Geosci. Remote Sens.* **1990**, *28*, 963–969. [CrossRef]
27. Fu, P.; Rich, P. Design and implementation of the Solar Analyst: An ArcView extension for modeling solar radiation at landscape scales. In Proceedings of the 19th Annual ESRI User Conference, San Diego, CA, USA, 26–30 July 1999.
28. Perez, R.; Ineichen, P.; Seals, R.; Michalsky, J.; Stewart, R. Modeling daylight availability and irradiance components from direct and global irradiance. *Sol. Energy* **1990**, *44*, 271–289. [CrossRef]
29. Palz, W.; Page, J.; Flynn, R.; Dogniaux, R.; Preuveneers, G.; Palz, W. *European Solar Radiation Atlas. Volume II, Global and Diffuse Radiation on Vertical and Inclined Surfaces*; Palz, W., Ed.; Verlag TÜV Rheinland GmbH: Köln, Germany, 1996.
30. Freitas, S.; Catita, C.; Redweik, P.; Brito, M.C. Modelling solar potential in the urban environment: State-of-the-art review. *Renew. Sustain. Energy Rev.* **2015**, *41*, 915–931. [CrossRef]
31. SciPy Documentation. Available online: https://docs.scipy.org/doc/scipy/ (accessed on 9 February 2022).
32. Oh, M.; Park, H.D. Optimization of solar panel orientation considering temporal volatility and scenario-based photovoltaic potential: A case study in Seoul National University. *Energies* **2019**, *12*, 3262. [CrossRef]
33. Yu, W.; Patros, P.; Young, B.; Klinac, E.; Walmsley, T.G. Energy digital twin technology for industrial energy management: Classification, challenges and future. *Renew. Sustain. Energy Rev.* **2022**, *161*, 112407. [CrossRef]
34. Deng, T.; Zhang, K.; Shen, Z.J. (Max) A systematic review of a digital twin city: A new pattern of urban governance toward smart cities. *J. Manag. Sci. Eng.* **2021**, *6*, 125–134. [CrossRef]
35. Francisco, A.; Mohammadi, N.; Taylor, J.E. Smart City Digital Twin-Enabled Energy Management: Toward Real-Time Urban Building Energy Benchmarking. *J. Manag. Eng.* **2020**, *36*, 04019045. [CrossRef]
36. Kakimoto, M.; Endoh, Y.; Shin, H.; Ikeda, R.; Kusaka, H. Probabilistic Solar Irradiance Forecasting by Conditioning Joint Probability Method and Its Application to Electric Power Trading. *IEEE Trans. Sustain. Energy* **2019**, *10*, 983–993. [CrossRef]
37. Libra, M.; Mrázek, D.; Tyukhov, I.; Severová, L.; Poulek, V.; Mach, J.; Šubrt, T.; Beránek, V.; Svoboda, R.; Sedláček, J. Reduced real lifetime of PV panels—Economic consequences. *Sol. Energy* **2023**, *259*, 229–234. [CrossRef]